International Journal of Heat and Mass Transfer 177 (2021) 121473

Contents lists available at ScienceDirect

International Journal of Heat and Mass Transfer

journal homepage: www.elsevier.com/locate/hmt

Impact of bed motion on the wall-to-bed heat transfer for powders in a rotary kiln and effect of built-ins

Gkiokchan Moumin[a,b,*], Stefania Tescari[a], Christian Sattler[a,b]

[a] Institute of Future Fuels, German Aerospace Center, Linder Hoehe, 51147 Cologne, Germany
[b] Chair of Solar Fuel Production, Institute of Power Engineering, Faculty of Mechanical Science and Engineering, TU Dresden, 01069 Dresden, Germany

ARTICLE INFO

Article history:
Received 8 February 2021
Revised 29 April 2021
Accepted 7 May 2021

Keywords:
Rotary kiln
Granular
Powder
Lifter
Rolling

ABSTRACT

This study analyses experimentally the heat transfer from the wall to the particle bed in a rotating drum with and without addition of built-ins for improving the mixing of the powder. Two types of materials were employed, sand as a granular material ($d_{p,mean} = 200\ \mu m$) and cement raw meal as a powdery material ($d_{p,mean} = 15\ \mu m$). A rotating cylinder heated through the outer shell was operated in batch mode, with rotational speeds of 1, 2 and 3 rpm and fillings of 5 and 10 %. The sand achieved a rolling motion, which makes the measured heat transfer coefficient predictable with theoretical models. At the contrary, cement raw meal showed very little mixing in a cylinder without built-ins and the measured heat transfer coefficient was much lower than the model predictions. Using longitudinal strips along the wall caused the powder to collapse regularly, increasing its heat transfer by a factor of 2–3, up to the range of predictions from theoretical models. Thus, a motion comparable to the rolling motion can be established with such built-ins which only cause limited dust formation. Furthermore, the limitations of the measurement method with rotating thermocouples are pointed out which mostly stem from the thermocouple response time and convectional losses, which are increased once built-ins are employed.

1. Introduction

Rotary kilns provide the possibility to treat different sizes and types of materials. Due to their flexibility, the application ranges nowadays from reduction of ores, calcination of limestone and petroleum coke through to waste treatment [1]. The kiln can be heated directly, i.e. the heat source is inside the kiln, or indirectly, where the heat source is not in contact with the treated material. The kilns are slightly tilted and the material is fed at the upper end. Through the rotation of the kiln, the material flows towards the outlet, while the flow behavior of solids is determined by their particle size.

Concerning the flowability, a threshold size of 100 µm can be defined, above which the particles are termed as granules and below as powders [2]. Granules show little cohesive forces and a thorough mixing of the bed can be established through the rotation of the kiln itself. While granules are superior in the handling and flowability, the treatment of powders is essential in industrial processes. An example for this is the cement production. The cement industry represents one of the biggest industrial CO_2 emitters, together with the steel industry, with each making up about 7 % of global emissions [3]. Half of these are process-related emissions from the calcination reaction performed at 900 °C [4].

However, powders show high cohesive forces and very little mixing in rotary kilns if no additional measures such as lifters are used. Aside from the homogeneity of the bed, the absence of mixing also affects the heat transfer into the material. Especially the heat transfer from the wall to the bed is directly correlated with the mixing of the bed. This heat transfer has been extensively studied in the literature for granules with several correlations being available. However, very few studies dealt with powders and their limitations regarding this. This aspect becomes all the more important, considering that the heat transfer from the wall to the bed is not negligible in the temperature range of 800–1100 °C [5,6]. Additionally, the bed motion affects the uptake of the radiative heat flow by several factors [7], with higher impacts at increased temperatures, which is the most important heat transfer mechanism at these conditions. Thus, the bed motion is a crucial parameter to shift the limiting heat transfer step from the bed surface to the gas temperature. Furthermore, previous studies observed the

* Corresponding author.
E-mail address: gkiokchan.moumin@dlr.de (G. Moumin).

https://doi.org/10.1016/j.ijheatmasstransfer.2021.121473

Nomenclature

Symbol	Description Unit
Latin	
A	Surface m^2
b	Thermal effusivity = $\sqrt{(\lambda^* \rho^* cp)}$ $J/(m^2\ K\ s^{0.5})$
F	Filling %
J	Radiosity W/m^2
$\tilde{M}$	Molar mass g/mol
$Q, \dot{Q}$	Heat, heat flow J, W
$R,\ r$	Radius m
$\bar{R}$	Gas constant = 8.314 J/(mol K)
$T, \bar{T}$	Temperature, time-averaged temperature K
a	Thermal diffusivity = $\lambda/(\rho \cdot c_p) m^2/s$
c_p	Specific heat capacity J/(kg K)
d_p	Particle diameter m
h, h^*	Bed height, fitting parameter m, 1/m
l	Modified mean free path of gas molecules m
m	Mass kg
n	Rotational speed rpm
s	Thickness m
t	Contact time s
Greek	
ϕ	Surface coverage factor –
α	Heat transfer coefficient $W/(m^2K)$
γ, γ^*	Filling angle, accommodation coefficient rad, –
δ	Roughness of particle surface m
ε	Emissivity –
λ	Thermal conductivity W/(m K)
ρ	Density kg/m^3
σ	Stefan-Boltzmann constant = $5.67 \cdot 10^{-8}$ $W/(m^2K^4)$
χ	Constant –
ω	Angular velocity rad/s
Index	
bed	Bed
cd	Conduction
con	Contact
cv	Convection
g	Gas
p	Particle, pressure
pen	Penetration
r	Radiation
rad	Radiation
s	Solid
w	Wall
wp	Wall to particle
ws	Wall to solid
Abbreviations	
CRM	Cement raw meal
TC	Thermocouple
TCP	Thermocouple plate

worse heat transfer with powders but they lack the identification of improvements through built-ins. Components, such as shovel-type lifters, are commonly used to enhance the heat transfer but this results in the formation of dust. However, low particle emissions are especially important in the field of concentrated solar thermal (CST) applications, which can provide the temperatures necessary for industrial processes but where reactors are mostly operated with a window or open to the atmosphere. The application of CST to powdery materials in solar rotary kilns is very limited [8] and the dust formation was found as an important question to solve in such systems [9]. Thus, it is not clear if minimally invasive built-ins such as longitudinal strips can improve the heat transfer to powders and to what extent.

2. Material and methods

2.1. Heat transfer in rotary kilns

The heat exchange in a rotary kiln consists of six main paths, involving radiative, convective and conductive heat exchange between the gas, wall and the bed (Fig. 2.1a). Although all these fluxes will be present for both a directly and indirectly heated kiln, the main heat source will be the gas for a direct operation and the wall for an indirect operation. Fig. 2.1b shows the geometric parameters defined to describe the kiln operation. The filling angle γ denotes the angle covered inside the kiln by the bed, h the bed height and l_γ is the circumference along which the wall and bed are in contact (covered wall).

There is no general rule on the importance of each heat transfer mechanism on the total heat transfer. As was summarized by Alonso et al., different studies found a varying influence of heat transfer by radiation and convection [10]. One of the reasons for this is the chosen experimental conditions: while Watkinson and Brimacombe [7] performed tests in a direct fired kiln with gas temperatures up to 830 °C, Barr et al. conducted tests with gas temperatures of about 1500 °C [5]. The results from Watkinson and Brimacombe showed that the main contribution to the heating of the bed through the gas is convection and that only 30 % of the heat is transferred by radiation from the gas. In contrast, results of Barr et al. illustrated a clear axial dependency of the heat transfer from the temperature. Although the heat transfer from the gas and the wall to the upper bed surface was dominant in most of the cases, the heat transferred by the covered wall to the bed underside still made up 12–25 % of the total heat flux in the case of limestone calcination in a kiln with refractory lining. Similarly, Gorog et al. showed that at gas temperatures of about 790 °C, 1080 °C and 1650 °C about 27 %, 13 % and 7 % of the total heat flow are provided from the wall to the bed, respectively [6].

The investigations by Watkinson and Brimacombe showed also the importance of the bed motion by varying the rotational speed and feeding rate, thereby the flow behaviour of the bed, and measuring its effect on the heat flux from gas to solids [7]. The bed movement, shown in a diagram as a function of rotational speed and filling, described different regions resulting in different degrees of mixing. The so-called bed behaviour diagram was later on extensively studied by Henein et al. [11]. Watkinson and Brimacombe found that the heat transferred from the gas to the solid increased by a factor of 2–4 if the mixing is increased. The higher

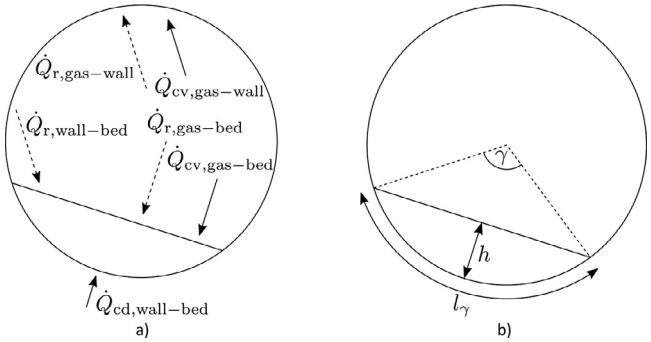

Fig. 2.1. Overview of the heat fluxes in a rotary kiln (a) and geometrical parameters (b).

values were found at higher gas temperatures. Therefore, the mixing of the bed is crucial for different heat transfer mechanisms. A direct indicator for determining if a bed is well mixed is to measure the heat transfer from the covered wall to the bed.

2.2. Wall-to-bed heat transfer

Different correlations have been established for the wall-to-bed heat transfer. These correlations can be separated in two types. The first, utilize a fully empirical correlation which is often only applicable to the studied or very similar conditions. This makes it difficult to compare the models with other works, leading to a limited application of them [12–14]. An exception is the model by Tscheng and Watkinson, which is a fit of prior published data, providing a simple yet accurate way to estimate the heat transfer coefficient [15]:

$$\alpha_{ws} = 11.6 \cdot \frac{\lambda_s}{l_\gamma} \left(\frac{\omega \cdot R^2 \cdot \gamma}{a_s} \right)^{0.3}, \tag{2.1}$$

with λ_s and a_s representing the thermal conductivity and thermal diffusivity of the solid bulk. The parameter ω represents the angular velocity and R radius of the cylinder. The filling angle γ is correlated to the filling F through:

$$F = \frac{\frac{\gamma}{2} - \sin\frac{\gamma}{2} \cdot \cos\frac{\gamma}{2}}{\pi}. \tag{2.2}$$

The second type of equations separates the heat transfer in two components: the heat transfer at the contact surface and the heat transfer inside the bulk. Inverting those allows the description through two resistances for the contact and penetration (Fig. 2.2).

The penetration heat transfer coefficient is derived through the contact of two surfaces and is described as [16]:

$$\alpha_{pen} = 2 \cdot \sqrt{\frac{\lambda_s \cdot \rho_s \cdot c_{p,s}}{\pi \cdot t}}. \tag{2.3}$$

The parameters λ_s, ρ_s and $c_{p,s}$ describe the thermal conductivity, density and specific heat of the bulk material. The parameter t describes the contact time, which is defined in rotary kilns through the rotational speed n and filling angle γ as:

$$t = \frac{\gamma \cdot 60}{2 \cdot \pi \cdot n}. \tag{2.4}$$

Thus, the penetration heat transfer is directly correlated to the filling and rotational speed, with lower fillings and higher rotational speeds leading to a higher heat transfer.

Where the models differ is the definition of the contact heat transfer coefficient. Most correlations include the particle size and gas thermal conductivity as main parameters. Some provide empirical values to account for the gap thickness between the wall and particle [12,17–19]. The most complete model is provided by Schlünder and Mollekopf, which separates the contact heat transfer in three parts [20]: conduction through wall-particle contact,

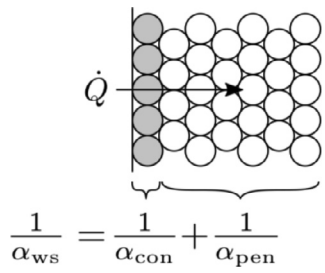

Fig. 2.2. Schematic representation of the contact and penetration resistance for the heat transfer from a wall to a particle bed adapted from Schlünder [16].

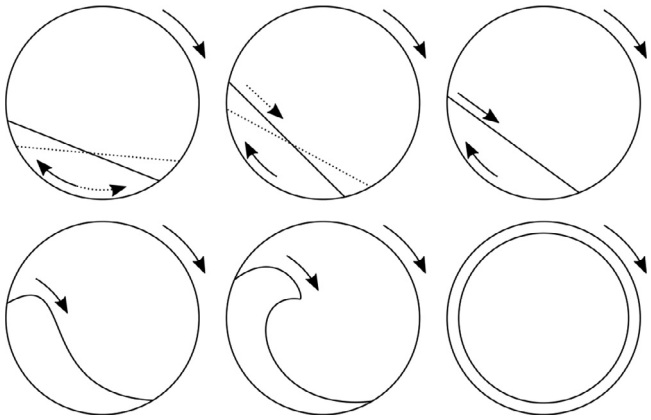

Fig. 2.3. Representation of the six bed motions (top, left to right) slipping, slumping, rolling, (bottom, left to right) cascading, cataracting and centrifuging, according to [11].

radiation wall-particle and heat transfer through the gas. Thus, parameters such as emissivities, surface roughness and surface coverage are included. Table 1 gives an overview of the correlations established for the heat transfer coefficients, which will be used to compare the experimental results obtained in this study.

2.3. Bed motion in rotary kilns

The heat uptake through wall contact correlates directly with the transversal bed motion which is distinguished in 6 types: slipping, slumping, rolling, cascading, cataracting and centrifuging, shown in Fig. 2.3 [11]. With increasing rotational speed and above a certain filling, the material motion transitions from a slipping and slumping motion into a rolling motion. This is generally considered as the ideal motion with maximized mixing [1]. Further increase in rotational speed results in tumbling motions, where attrition is increased, up to the centrifuging motion. However, it is important to note that these motions are only valid for granular material. Powdery material cannot be operated in a rolling motion, which results either in motions where mixing is almost absent (slipping, slumping) or only irregular (cascading, cataracting).

2.4. Heat transfer analysis of powders

Out of the 15 studies reviewed from literature on wall-to-bed heat transfer, only 3 employed powders. Out of those, two used a smooth cylinder [13,22] and one a cylinder with flights [21]. Pashkevich analysed the heat transfer to a powder at fillings of 20 and 40 % [13]. Rotational speeds were up to 19 rpm, covering all bed motion types up to a centrifuging motion. An empirical correlation was provided and no comparison with literature models was done. Herz et al. were in 2015 the first to compare the impact of different bed motions on the heat transfer coefficient [22]. While material in rolling motion agreed with the predictions from literature, slumping and sliding motions led to an overestimation of the heat transfer coefficient through the models by a factor of 3 and 5. Wes et al. utilized 9 shovel-type built-ins which resulted in measured heat transfer coefficients in agreement with the penetration heat transfer coefficient [21]. Thus, the contact resistance was found to be negligible which agrees with values calculated for the contact heat transfer for powders from the Schlünder and Mollekopf model.

This review shows that studies on powders are lacking and, more importantly, that no study exists which quantifies the improvement through the usage of built-ins such as longitudinal strips. Only the two extreme cases of a cylinder without or with

Table 1
Overview of established correlations for the heat transfer coefficient wall-to-bed.

Author	Correlation
Wachters and Kramers 1964 [12]	$\alpha_{ws} = \left(\frac{\sqrt{\pi}\cdot d^*}{2\cdot\lambda_s} + \frac{1}{\alpha_{pen}}\right)^{-1}$ for < 9.5rpmwith $d^* = \sqrt{\gamma}\cdot 1.12\cdot 10^{-3}\alpha_{ws} = \frac{\alpha_{pen}}{3}$ for > 9.5rpm
Sullivan and Sabersky 1975 [17]	$\alpha_{ws} = \left(\frac{\chi\cdot d_p}{\lambda_g} + \frac{1}{\alpha_{pen}}\right)^{-1}$ with $\chi = 0.085$
Wes et al. 1976 [21]	
Lehmberg et al. 1977 [18]	$\alpha_{ws} = \alpha_{pen} - \frac{b_s}{\sqrt{t}}\left(\frac{1}{h^*\cdot\sqrt{a_s\cdot t}} + \frac{1}{h^*\cdot\sqrt{a_s\cdot t}}\cdot\exp(h^{*2}\cdot a_s\cdot t)\cdot\mathrm{erfc}(h^*\cdot\sqrt{a_s\cdot t})\right)$ with $h^* = 3607\,\frac{1}{m}$ for sand with $d_p = 157\ \mu m$
Tscheng and Watkinson 1979 [15]	$\alpha_{ws} = 11.6\cdot\frac{\lambda_s}{l_\gamma}\left(\frac{\omega\cdot R^2\cdot\gamma}{a_s}\right)^{0.3}$
Schlünder and Mollekopf 1984 [20]	$\alpha_{ws} = \left(\frac{1}{\alpha_{con}} + \frac{1}{\alpha_{pen}}\right)^{-1}$ with$\alpha_{con} = \phi\cdot\alpha_{wp} + (1-\phi)\cdot\frac{2\cdot\lambda_g/d_p}{\sqrt{2}+\frac{2.1+2.3}{d_p}} + \alpha_{rad} + \alpha_{dir}$ see Appendix A.1 for explanations
Li et al. 2005 [19]	$\alpha_{ws=}\left(\frac{\chi\cdot d_p}{\lambda_g} + \frac{1}{\alpha_{pen}}\right)$ with $\chi = 0.1$

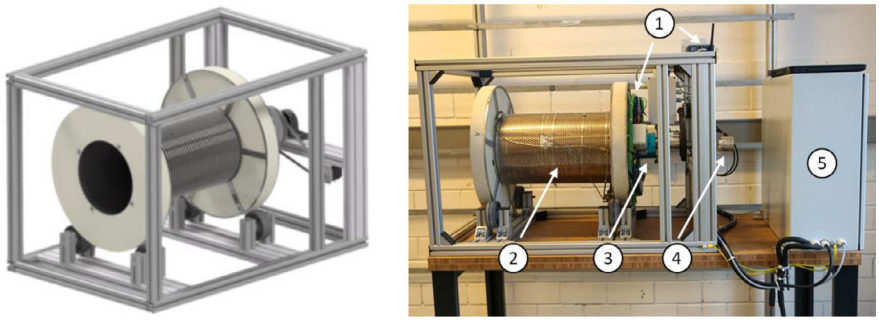

Fig. 3.1. (a) CAD-drawing of the setup and (b) side view with the components: (1) Wi-Fi-modules, (2) heating cable, (3) slip-ring assembly, (4) rotary encoder and (5) control cabinet.

built-ins were analysed, missing a direct comparison of both conditions.

3. Experiments

3.1. Description of setup

An indirectly heated rotary kiln operated in batch mode is used for the heat transfer analysis. The side view of the setup without insulation is shown in Fig. 3.1a and b. The cylinder is made of stainless steel (1.4404) and has a diameter of 250 mm, length of 500 mm and thickness of 2 mm. The small thickness was chosen to reduce the thermal inertia of the cylinder and to have a fast response time of the setup. The front of the setup is closed with transparent acrylic glass, allowing the observation of the bed motion. The heat is applied uniformly to the external wall through a heating cable which is wrapped around the cylinder and can supply a maximum power of 6.5 kW.

In total, 33 K-type thermocouples with diameters of 0.5 mm are mounted on the setup, 30 inside the cylinder and the remaining 3 at the front, back and between the outer shell and the heating cable to provide a temperature for controlling its operation. The data acquisition is done with Wi-Fi modules and the power input to heat the rotating part of the setup is established with a slip-ring assembly. A rotary encoder is mounted at the end of the shaft to obtain the angular position of the cylinder.

3.2. Temperature measurement

In general, the temperature measurement inside a rotary cylinder can be established with thermocouples which are rotating with the cylinder or maintained at a fixed position inside the particle bed. The advantage of the fixed position is the reduced response time while the rotating thermocouples allow the measurement of temperatures along the circumference outside of the bed. Sonavane compared the measured temperatures with both methods at a rotational speed of 8 rpm in a bed of quartz sand [23]. No significant

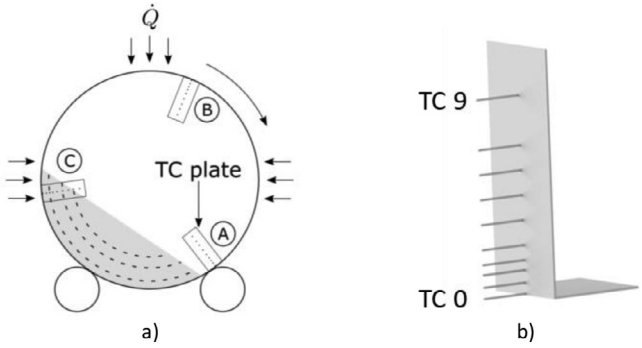

Fig. 3.2. (a) Schematic view of the setup with the three measurement plates and (b) representation of the thermocouple alignment on a plate.

difference was found and the author utilized the rotating thermocouples for the calculations.

The thermocouples inside the present cylinder are fixed at the wall on radially distributed L-shaped plates, referred to as thermocouple plates (TCP). In total, 3 plates are mounted at the half length of the cylinder, referred to as TCP A–C and shown in Fig. 3.2a.

The thermocouples protrude 10 mm out of the plates to avoid any influence of the plate temperature on the measurement and are arranged vertically at the positions 0, 2.5, 5, 7, 10, 15, 20, 25, 30 and 40 mm from the wall (Fig. 3.2b). Due to strong noise induced by the heating cable, the data is acquired every second in the low-speed acquisition mode, as this incorporates a noise rejection.

3.3. Procedure and materials

The experiments were performed with the following procedure:

1) Filling of the cylinder with material and closing it
2) Starting of data recording and rotation

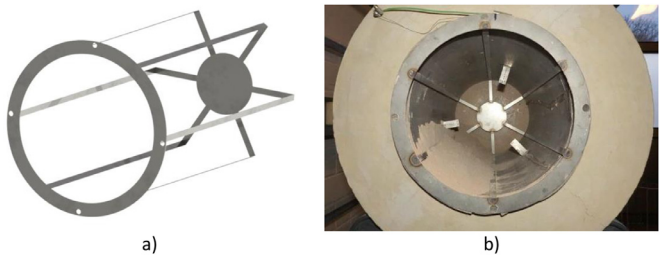

Fig. 3.3. (a) Drawing of built-in with 6 strips used to induce mixing of the CRM and (b) front view of the setup with inserted built-in.

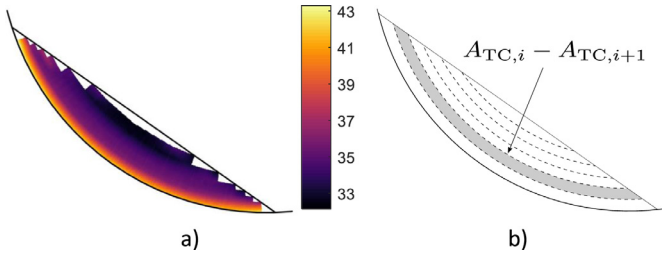

Fig. 3.4. (a) Measured radial temperature distribution inside the bed and (b) exemplary view of the area allocation to calculate the average bed temperature. Values are given in °C.

3) Setting the heater to the target temperature of 120 °C with a power input of 1.1 kW
4) Stop of experiment once the wall reaches the target temperature

Two types of particles were used: Quartz sand with a size of 100–300 µm and industrial cement raw meal (CRM) with a size of <176 µm. The bulk densities of the particles were determined according to the method of measuring the weight of a defined volume of material (EN ISO 60). The effective thermal conductivities of the bulks were measured at room temperature with the Hot Disk TPS 2500 S and are considered to be constant in the analysed temperature range. The specific heat capacities were obtained through the literature [24,25]. The analysed fillings were 5 and 10 %, whereas the rotational speeds were 1, 2 and 3 rpm.

For the analysis of the heat transfer to the CRM, a further distinction is necessary. As discussed in section 2.3, the mixing of the CRM has to be established with built-ins. Therefore, longitudinal strips were used as a minimally invasive option. The strips showed a good performance in prior cold observation tests. The height of the strips was chosen as 2 mm. A grid-like structure is used, which can be fixed to the front of the cylinder to establish contact of the strips with the wall and represent therefore an obstacle for the CRM particles and induce a mixing. The built-in with 6 strips is shown separately and mounted inside the setup in Fig. 3.3a and b. A slightly convex structure ensures the contact of the strips with the wall and the additional surface of the strips is considered in the calculations as an increase in the heat transfer area.

Thus, on one hand the heat transfer between a smooth cylinder and the CRM particle was analysed. On the other hand, the enhanced heat transfer with strips was measured. Two built-ins, one with 6 strips and one with 12 strips were used.

The properties of the materials and the analysed experimental conditions are given in Table 3.1.

The heat transfer coefficient from the wall to the bed is determined through an energy balance of the bed including the heat transferred from the wall ($\dot{Q}_{ws}$) and losses due to radiative heat exchange of the bed with the front, back and inner surfaces of the cylinder ($\dot{Q}_{rad}$):

$$\dot{Q}_{ws} - \dot{Q}_{rad} = \dot{Q}_{bed}, \tag{3.1}$$

and

$$\alpha_{ws} \cdot A_{ws} \cdot (T_w - T_s) - \dot{Q}_{rad} = m_s \cdot c_{p,s} \cdot \frac{dT_s}{dt}. \tag{3.2}$$

The heat transfer coefficient from the wall to the bed follows as:

$$\alpha_{ws} = \frac{m_s \cdot c_{p,s} \cdot \frac{dT_s}{dt} + \dot{Q}_{rad}}{A_{ws} \cdot (T_w - T_s)}. \tag{3.3}$$

This approach is similar to that followed by Sonavane, Herz et al. and Nafsun et al., while the authors did not include the radiative exchange as a term for the energy balance [22,23,26–31]. The radiative heat exchange is considered in this case through a radiation network according to Bergman et al. [32].

3.4. Temperature of the bed

The bed temperature T_s is obtained by area-weighted averaging of the values measured by the thermocouples passing through the bed. To determine the contribution of each position to the average bed temperature, the profile inside the bed was obtained once in the high-speed acquisition mode. To avoid the strong noise induced by the heater, the heating was disabled for the time span of measurement. The rotation was set to 1 rpm, sand was used as the bed material and a rolling motion was obtained. The result of the measurement is given in Fig. 3.4a.

The highest temperatures can be seen at the wall, whereas the lowest temperatures are found in the upper core of the bed. This distribution is similar to a fixed bed and was confirmed by visual observation, where only a thin active layer on the top of the bed was seen with enhanced mixing among the particles. The movement of the remaining volume was similar to a fixed bed, where no mixing takes place. Each area is calculated with:

$$A_{TC,i} = \frac{r_i^2}{2} \cdot (\gamma_i - \sin \gamma_i), \tag{3.4}$$

and

$$\gamma_i = 2 \cdot \operatorname{acos}\left(1 - \frac{(h - s_i)}{r_0 - s_i}\right), \tag{3.5}$$

with r_i being the radial position of the respective thermocouple, γ_i the filling angle at the respective position, h the height of the bed and s_i the distance of the respective thermocouple from the wall.

Table 3.1
Properties of used particles and experimental parameters for the heat transfer analysis.

	Quartz sand	Cement raw meal
Particle size, mean (µm)	100–300, 200	<176, 15
Bulk density at 20 °C (kg/m³)	1397	932
Specific heat (J/kg/K)	$782 + 0.571 \cdot (\frac{T}{K}) - 1.881 \cdot 10^7 \cdot (\frac{T}{K})^{-2}$ [24]	$880 + 0.293 \cdot (\frac{T}{°C})$ [25]
Effective thermal conductivity at 20°C (W/m/K)	0.27	0.14
Rotational speed (rpm)	1, 2, 3	1, 2, 3
Filling (%)	5, 10	5, 10
Number of strips	0	0, 6, 12

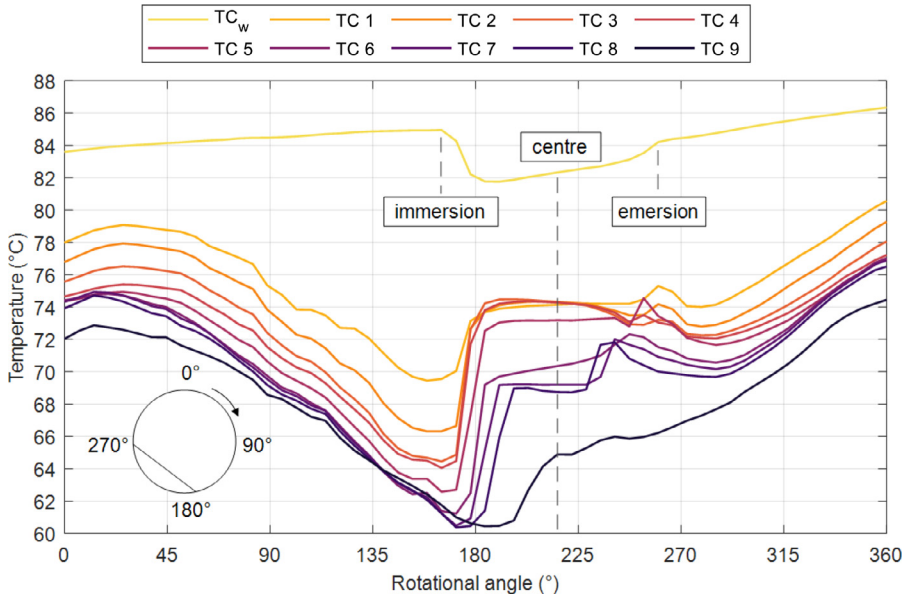

Fig. 3.5. Detailed view of the temperatures recorded at plate A during a full rotation. The immersion of the plate into the bed, the centre of the bed and the emersion of the plate out of the bed are marked.

Subsequently, the temperature of the whole bed is calculated as:

$$T_s = \frac{1}{2 \cdot A_{bed}} \sum_i (A_{TC,i} - A_{TC,i+1}) \cdot (T_{TC,i} + T_{TC,i+1}), \tag{3.6}$$

Where A_{bed} represents the cross-sectional area of the bed. A schematic view of the respective area between TC_i and TC_{i+1} is given in Fig. 3.4b. Thus, at the position of each thermocouple a circular segment is defined, Eq. (3.4), while the respective filling angle at the considered thermocouple position is obtained with Eq. (3.5). By subtracting from the segment area of TC_i, covering the area from the cord length to the lower side of the grey area in Fig. 3.4b, the segment area of TC_{i+1}, the grey marked area is obtained. For this area, the average of both enclosing temperatures is allocated. The sum of this process for the whole bed is represented in Eq. (3.6).

3.5. Exemplary case

The determination of the heat transfer coefficient will be discussed in detail for a case with 10 % filling of sand particles, rotated at 1 rpm. Fig. 3.5 shows the temperatures recorded at plate A during a full rotation. The angles 0° and 180° denote the positions where the plate is at the top and bottom of the cylinder, respectively. The pattern shown here for a full rotation at the measurement plate A was similar for all three plates.

From these profiles, the wall and bed temperature over the experimental time can be obtained, as shown in Fig. 3.6 for the thermocouple plate A. The temperature of the bed is calculated according to Eq. (3.6) using temperatures at different heights at the bed centre.

Fig. 3.6 shows that the temperature difference between the wall and the bed initially increases to a maximum, 10 minutes after the start of the experiment, and decreases afterwards. This difference stays in the range of 5–12 °C during the whole experiment.

Considering the temperature data from each rotation, the calculated heat transfer coefficient according to Eq. (3.3) is shown in Fig. 3.7. A wide range from $64 - 184 W/(m^2K)$ is found while the values at all plates show a constant trend during the experiment. The total average is found to be $136.5 W/(m^2K)$. Two things can be noted: First, the values at plate C are lower than those at

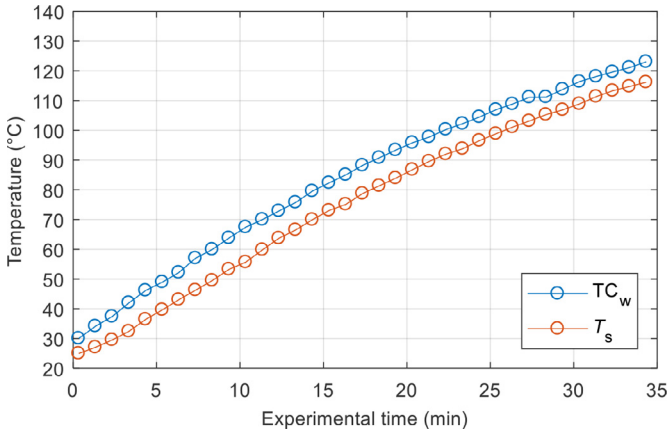

Fig. 3.6. Recorded wall and average bed temperature at plate A during a test with 10 % sand at 1 rpm.

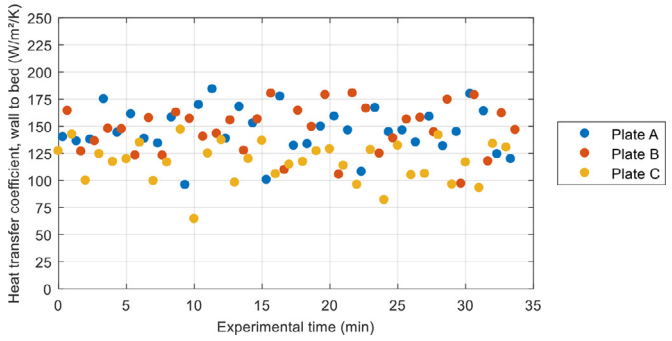

Fig. 3.7. Heat transfer coefficient for the case with 10 % sand at 1 rpm.

A and B. Repeated tests showed, that the wall temperatures have constant deviations among the plates. This was likely caused by a non-uniform contact of the heating cable on the outer cylinder surface, as was measured with radially distributed thermocouples on the inner wall. Therefore, the wall temperatures were fitted to have a correct representation of the temperature along the circumference (Fig. 3.8). Second, a strong fluctuation of the coefficient for all plates can be seen.

This is due to the fact, that the coefficient is sensitive to the variation of the bed temperature (see Eq. (3.3)). Although the bed temperature increases steadily, it is clearly visible that the increase is not constant (see Fig. 3.6).

One example for this is the bed temperature measured after minute 10, which is only slightly higher than before (see Fig. 3.6). Thus, the heat transfer is calculated to be exceptionally low, as can be seen in Fig. 3.7 for plate A before minute 10. On the contrary, the next value is on the other extreme of the scale.

This behaviour is system inherent, since although the bed is in a rolling motion, slight transversal oscillations are always present, leading to differences in the measurements. Looking at the previously reviewed literature, only some of the studies report the heat transfer coefficient vs. time or temperature [14,22,23,26–31]. The majority states only a single value for the coefficient, thus averaging the term over the whole experiment. Considering the bed motion behaviour and the validity of assuming a steadily heating bed, an averaging of the heat transfer coefficient over multiple measurements instead of the whole experiment is performed in this study. For cases at 1 rpm, the coefficient is calculated over 5 measurements at each plate, whereas for 2 and 3 rpm the number of included measurements is increased to 9 and 13, respectively. This results in a time span of 4 minutes for each case.

The heat transfer coefficients calculated with the averaging and fitted wall temperature are shown in Fig. 3.8. A good agreement between the three plates can be seen, with deviations being in a range of +10 % to −11 %. The average value for each plate is 132, 139 and 134 W/(m²K), respectively. Thus, after the averaging over multiple measurements, to avoid the random fluctuations (Fig. 3.7), and the fitting of the wall temperatures, to avoid the systematic deviation of plate C from A and B (Fig. 3.7), the evaluation of the data is possible.

4. Results and discussion

4.1. Validation of the setup

A comparison of the heat transfer coefficient α_{ws} obtained with literature models is done for sand at a filling of 10 % and at 1 rpm. Fig. 4.1 shows the heat transfer coefficient vs. bed temperature for the experiment and calculated values from 7 models discussed in section 2.2. The average α_{ws} of the three plates is shown as a solid line whereas the total range from all three plates is shown as a cloud.

The measurements agree well with most of the models up to a solid temperature of 80 °C. An exception is the model by Wachters and Kramers which predicts much lower values. The model is based on a single particle size and therefore the empirical fit is not applicable to other cases. The remaining models predict an increase of the heat transfer with increasing temperatures, due to an increase of the specific heat of the bed and the thermal conductivity of the air, which is not found for the experimental values. Further tests have shown that this deviation becomes bigger for lower fillings and especially when strips are used with the CRM. This behaviour will be addressed in a subsequent section. Furthermore, it has to be remarked, that the assumption of a constant thermal conductivity will lead to an underestimation of the calculated coefficients at elevated temperatures.

For most of the subsequent tests it was seen that the model results from Wes et al. and Tscheng and Watkinson represent the upper and lower range of the predicted values. Similarly, it was found that the model by Schlünder and Mollekopf predicts the highest value of all models incorporating the contact resistance. The model by Wachters and Kramers was found to highly underestimate the heat transfer in most cases and is therefore neglected. Thus, all subsequent comparisons will include the models of Wes et al., Tscheng and Watkinson and Schlünder and Mollekopf which already allow putting the results in perspective to the literature values.

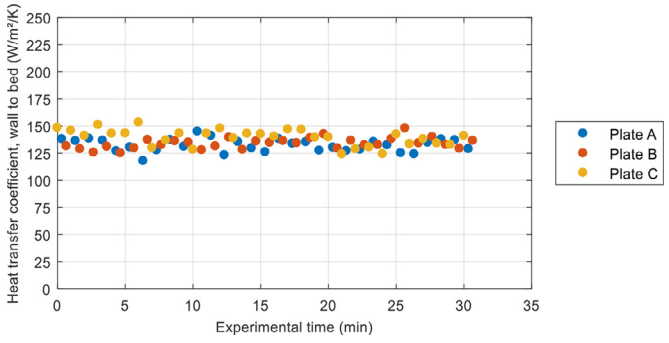

Fig. 3.8. Heat transfer coefficient for the case with 10 % sand at 1 rpm with averaging over 5 measurements and fitting of the wall temperature.

4.2. Experimental results

First, the measured heat transfer coefficients in dependence of the bed temperature will be compared with literature values. For all cases with sand, a rolling motion was established inside the cylinder. Fig. 4.2 shows the average obtained for sand at fillings of 5 and 10 % and rotational speeds of 1–3 rpm. A good agreement is found at a rotational speed of 1 rpm at both fillings (Fig. 4.2a and d). However, the rising trend predicted by the models is not found in the experiments. An increase of the rotational speed to 2 rpm shows a satisfactory agreement with the predictions below 80 °C for a filling of 5 % (Fig. 4.2b). With a filling of 10 % a better agreement is found and only a slight decrease over the whole range is visible (Fig. 4.2e). The models predict higher heat transfer coefficients compared to the 1 rpm cases since the increased rotation enhances the penetration of the heat into the bed.

A further increase in the rotational speed results in a linearly decreasing profile for the experimental values in the case with low filling (Fig. 4.2c). However, up to a bed temperature of 50 °C the range overlaps with the model by Tscheng and Watkinson. At the higher filling the experimental values lie always in the range of the models, although a decreasing trend is also found in this case (Fig. 4.2f). It is also observed that the predictions between the literature models differ stronger with higher rotational speed. This is due to the different consideration of the contact resistance, caused by the interstitial gas (see Table 1).

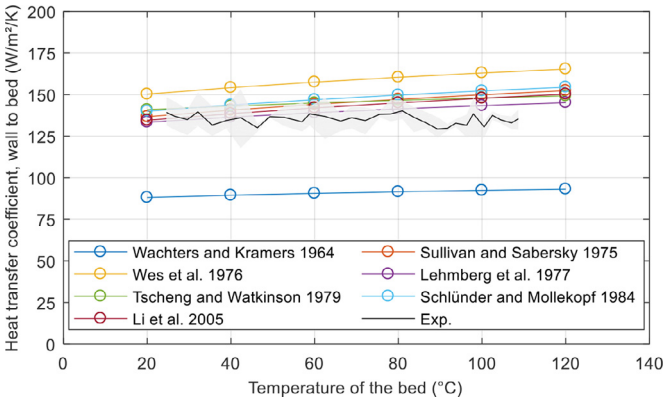

Fig. 4.1. Comparison of experimentally measured heat transfer coefficient with literature models for the case with 10 % sand rotated at 1 rpm. The average experimental value together with the obtained range at all plates is given.

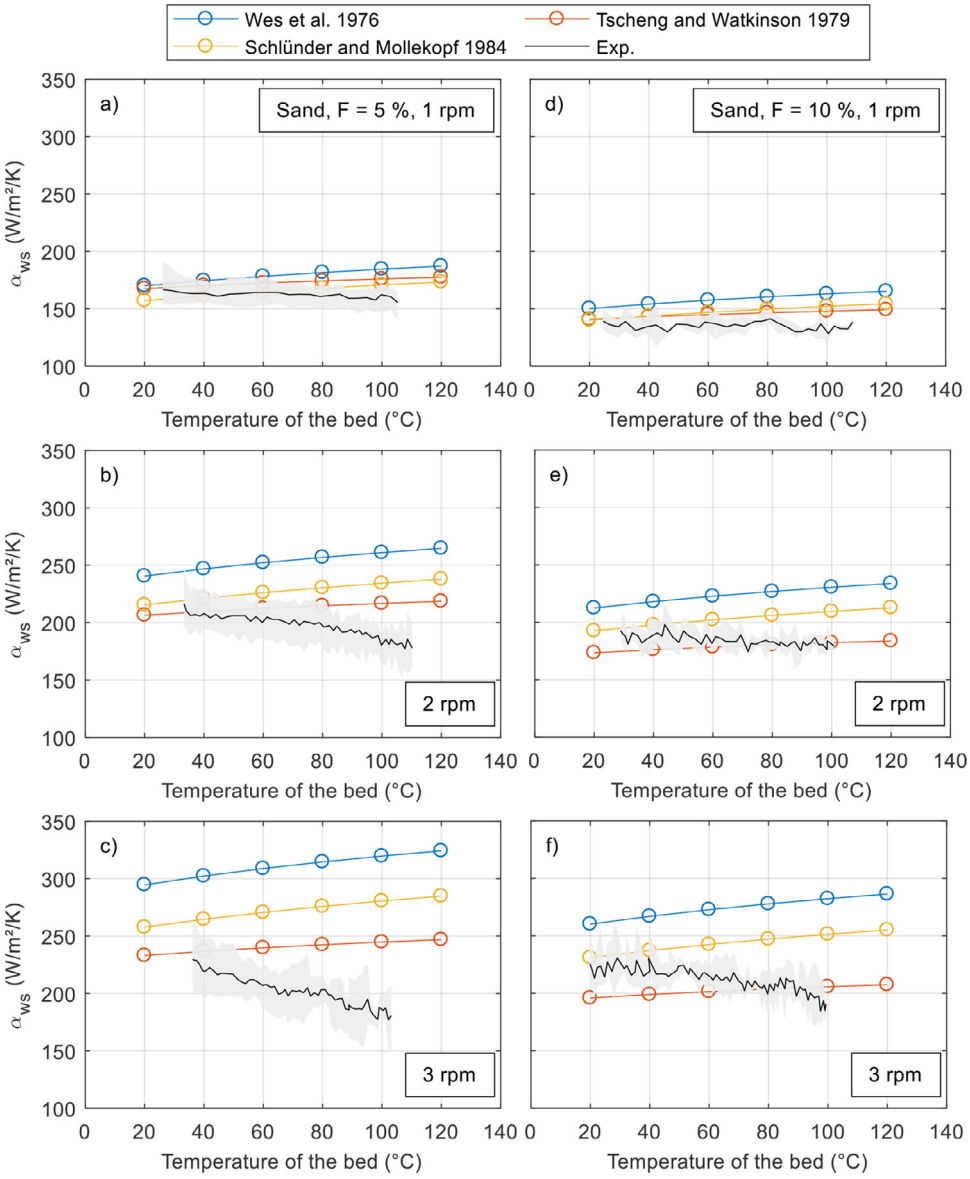

Fig. 4.2. Measured heat transfer coefficient versus bed temperature for sand at fillings of 5 % (a–c) and 10 % (d–f) and rotational speeds of 1–3 rpm.

For the CRM, first the experiments in the cylinder without strips are discussed (Fig. 4.3, black lines). As expected, a sliding motion was established inside the cylinder and the measured values are always much lower than the model predictions (Fig. 4.3a–f). An increase of the rotational speed does not significantly affect the measured heat transfer coefficient. Considering all experiments, the values are up to a factor of 6 lower than the calculated ones.

This is in line with the values reported by Herz et al., who found lower heat transfer coefficients due to the sliding motion up to a factor of 5 [22].

Interestingly, the predictions from the Schlünder and Mollekopf model for the CRM agree with those from Wes et al. This can be explained with the small mean diameter of the CRM particles of 15 µm. With such a particle size, the resistance induced by the interstitial gas becomes negligible. Therefore, models including this resistance agree with the predictions of the model by Wes et al., which only considers the heat penetration into the bed. This was also found for the other models, which are not shown in the graph. The model by Tscheng and Watkinson is an empirical fit of experimental results and does not include the particle size as a parameter. Therefore, it is not affected by the small particle size of the CRM.

The results with the CRM demonstrate, for improving the heat transfer coefficient mixing has to be induced in the bed. Once the strips are inserted in the cylinder, the heat transfer is highly improved.

For all rotational speeds, the heat transfer coefficient measured with 6 or 12 strips is initially in agreement with the literature models (Fig. 4.3, blue and orange lines without circles). Interestingly, no significant difference between the usage of 6 strips and 12 strips is seen although prior visual observations hinted at a stronger mixing with 12 strips. Contrary to the smooth cylinder, an increase of the rotational speed results in an increase of the heat transfer coefficient. Again, it is found that the measured heat transfer coefficient decreases with increasing bed temperature. This behaviour will be further discussed in section 4.3.

Lastly, the results obtained with both materials in dependence of the rotational speed are summarized. The comparison with literature data is done at a solid temperature of 40 °C, since some

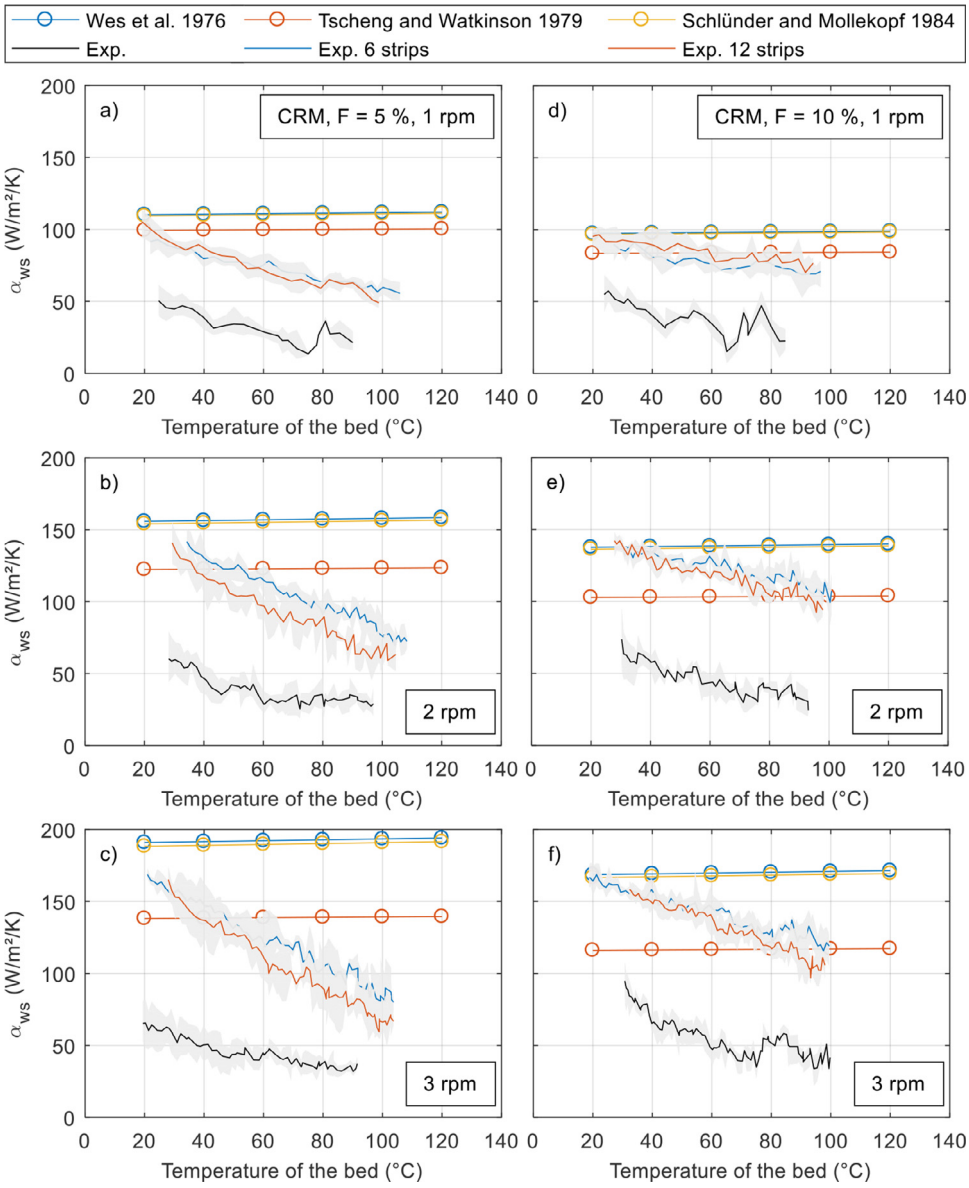

Fig. 4.3. Measured heat transfer coefficient versus bed temperature for CRM at fillings of 5 % (a–c) and 10 % (d–f) at rotational speeds of 1–3 rpm and without, with 6 and with 12 strips.

tests were only started above 30 °C and to limit the effect of the temperature shown previously.

The heat transfer coefficients for sand and CRM at a filling of 5 % are summarized in Fig. 4.4. The dots represent the average of all 3 plates and the error bars represent the standard uncertainty according to the GUM [33]. The details on the uncertainty calculation can be found in the Appendix A.2. The comparison shows, that the predicted and measured values for sand are higher than those for the CRM.

This is due to the difference in the thermal properties of the materials. While sand has a comparatively low specific heat capacity, both its thermal conductivity and density are relatively high. Thus, the thermal effusivity $\sqrt{\lambda_s \cdot \rho_s \cdot c_{p,s}}$, which is the key parameter for the penetration heat transfer coefficient, is significantly higher. The results for CRM at 1 rpm and without strips are about 2.5 times lower than the predicted values. With increasing rotational speed, the deviation from the predictions rises up to a factor of 4. This is expected, due to the unchanging bed motion.

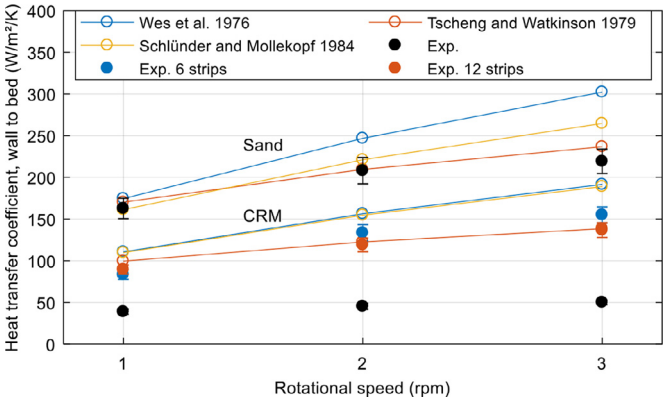

Fig. 4.4. Heat transfer coefficient for sand and CRM at a filling of 5 % and at 40 °C. Results for CRM include the cases without strips, with 6 and 12 strips. The average value of the 3 plates is shown, with the bars representing the uncertainty.

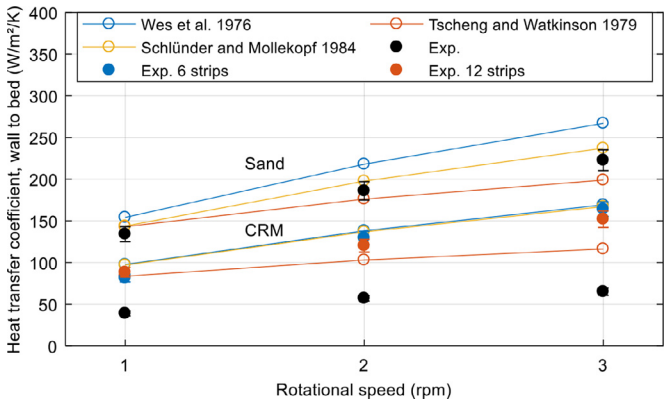

Fig. 4.5. Heat transfer coefficient for sand and CRM at a filling of 10 % and at 40 °C. Results for CRM include the cases without strips, with 6 and 12 strips. The average value of the 3 plates is shown, with the bars representing the uncertainty.

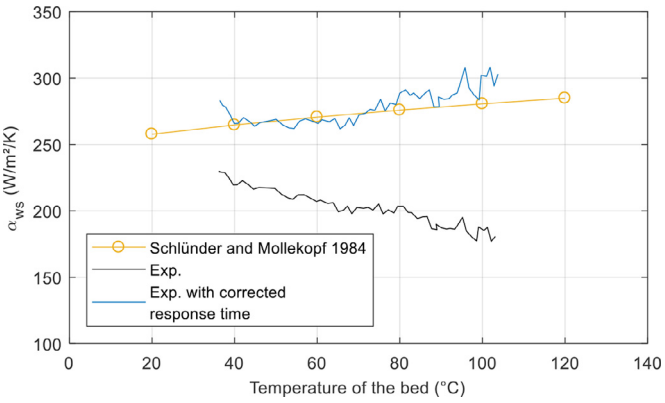

Fig. 4.6. Heat transfer coefficient for sand at 5 % filling and 3 rpm. Average experimental values are given calculated from the raw data (black line) and corrected data (blue line) by assuming the recorded bed temperature being 98 % of the actual temperature.

The increase in the heat transfer coefficient with the strips in comparison to the model values gives an indication of how close the bed is to a theoretical rolling motion. After inserting the built-in with 6 strips, a significant increase in the heat transfer is visible. Improvements by a factor of 2.2, 2.9 and 3.1 can be seen for the respective rotational speeds. Since the bed motion is now directly affected by the rotational speed, an increase of the heat transfer coefficient together with the rotation is found.

Fig. 4.5 summarizes the results at a filling of 10 %. Again, the values for sand show a good agreement with the model predictions. For the CRM, the implementation of strips increases the heat transfer coefficient by a factor of about 2 for all rotational speeds. It can also be seen, that the improved heat transfer is closer to the values predicted by the penetration theory (described by Wes et al.). Again, no significant difference between the usage of 6 strips to 12 strips is visible. However, it cannot be concluded that lower numbers of strips would yield the same effect since a minimum number will be required to achieve a motion similar to a rolling motion. The studied range does not allow to determine this number conclusively.

4.3. Sensitivity to temperature

Comparison of the obtained profiles for the heat transfer coefficient vs. the bed temperature with other experimental work is only possible with Sonavane, Herz et al. and Nafsun et al. [22,23,26–31], since no other work includes the temperature dependency. Although Bongo Njeng et al. report the heat transfer coefficient over the experimental time, their study was performed in a continuous operation with temperatures maintained constant [14]. Thus, the authors found a constant value for the heat transfer coefficient over time which is to be expected due to the constant experimental boundary conditions.

In the work from Sonavane, the heat transfer coefficient is measured as constant or even decreasing during the experiment [23]. The decrease is stronger at lower fillings and higher rotational speeds, similar to what was observed in this study. Similarly, Herz et al. and Nafsun et al. report in their studies only constant or decreasing heat transfer coefficients over the experimental time [22,26–31]. The effect in all of these studies is not as severe as presently observed for the case with the CRM together with the built-ins. This can be attributed to the fact that the fillings in the reported studies were in the range of 10–20 % and no built-ins were used.

The reduction of the filling and increase of the rotational speed have two main effects: First, the thermocouples have less time to match the actual bed temperature. Although the thermocouples have a diameter of only 0.5 mm, the response time will become more significant with increasing rotational speeds. The temperature difference between wall and bed decreases over the experiment and thus, small deviations in the temperatures have a stronger effect on the measured heat transfer coefficient (denominator in Eq. (3.3)). Indeed, the comparison by Sonavane of temperatures measured by a rotating and fixed thermocouple at 8 rpm with 10 % filling shows that although the temperatures are close, the values from the rotating one were mostly lower by 1 °C [23]. If it is considered, that in the present case the measured bed temperature is only 98 % of the actual temperature, the result for the case with sand at 5 % filling and 3 rpm shows a good agreement with the predictions from the model by Schlünder and Mollekopf, as shown in Fig. 4.6. For the other analysed cases with sand, lower deviations were always found at lower rotational speeds. However, this effect alone could not explain the results with the CRM, especially once the strips were used.

The second effect of the higher rotation and especially with the strips is the increased convectional heat exchange with the air inside the cylinder. Looking at the gas temperatures above the bed surface it was in fact seen, that the difference between the bed and gas temperature increases during the experiment. This would result in higher convectional losses from the surface of the bed with the progress of the experiments. Estimations of the convectional heat transfer showed that this heat flux is by an order of magnitude too small to explain the effect, if a smooth bed surface is considered. However, in the case of the CRM with strips, the bed is not a smooth surface and, more importantly, the regular collapses of the bed cause the air to enter into the bulk. Thus, the heat exchange is vastly improved which would require to incorporate the convectional losses into the balance to have accurate results for the heat transfer coefficient (Eq. (3.3)). Estimations showed that these losses are in a reasonable range and a good agreement with literature predictions could be established once they were included. Hence, the increased convective losses could explain the observed deviations for the cases with CRM.

5. Conclusions

The heat transfer to the bed inside a rotary kiln is directly correlated to the bed motion. For granules (>100 µm), sufficient mixing can be established by the rotation of the kiln itself. However, powders require additional measures such as the usage of built-ins inside the kiln. While this was known, studies were missing comparing the operation without and with built-ins to quantify the possible improvement. In this work, an indirectly heated cylinder in batch operation was used to fill this gap. One granular material, sand with a mean size of 200 µm, and one powdery mate-

rial, cement raw meal (CRM) with a mean size of 15 µm, were employed. Rotational speeds of 1, 2 and 3 rpm were set together with fillings of 5 and 10 %. As expected, the measurements with the sand were in accordance with literature models. Once the CRM was analysed, the wall-to-bed heat transfer coefficient at 40 °C was up to 4 times lower than the predictions. Inserting 6 or 12 longitudinal strips increased the heat transfer coefficient by a factor of 2–3, up to the range of the values predicted by literature models for a rolling motion. Taking the study from Watkinson and Brimacombe as a reference [7], this established rolling will improve the radiative heat transfer in the same order of magnitude. Thus, such strips represent an efficient solution for heat transfer enhancement in rotary kilns while ensuring a low dust formation. During the trials it was observed that the measured heat transfer coefficient decreased with increasing bed temperature, while model predictions showed the opposite behaviour. This decrease was stronger with lower fillings and higher rotational speeds. Analyses showed that the response time of the thermocouples and the convectional losses induced by the strips are the main factors for this deviation.

Declaration of Competing Interest

The authors declare that they have no known competing financial interests or personal relationships that could have appeared to influence the work reported in this paper.

CRediT authorship contribution statement

Gkiokchan Moumin: Conceptualization, Methodology, Investigation, Formal analysis, Writing – original draft. **Stefania Tescari:** Conceptualization, Writing – review & editing, Supervision. **Christian Sattler:** Writing – review & editing, Supervision.

Acknowledgements

This project has received funding from the European Union's Horizon 2020 research and innovation programme under grant agreement No. 654663, SOLPART project.

Appendix

A.1. Contact heat transfer coefficient by Schlünder and Mollekopf

The coefficient is dependent on the heat transfer to a single particle α_{wp}, heat transfer through the gas and heat transfer via radiation α_{rad}:

$$\alpha_{con} = \phi \cdot \alpha_{wp} + (1-\phi) \cdot \frac{2 \cdot \lambda_g / d_p}{\sqrt{2} + \frac{2 \cdot l + 2 \cdot \delta}{d_p}} + \alpha_{rad}, \tag{A.1}$$

with ϕ representing the surface coverage factor being mostly about 0.8, d_p the particle diameter, l the modified mean free path of the gas molecules and δ the roughness of the particle surface [20]. The heat transfer to a single particle is described as follows:

$$\alpha_{wp} = 4 \cdot \frac{\lambda_g}{d_p} \left(\left(1 + 2 \cdot \frac{l+\delta}{d_p} \right) \ln \left(1 + \frac{d_p}{2 \cdot (l+\delta)} \right) - 1 \right), \tag{A.2}$$

with

$$l = 2 \cdot \frac{2-\gamma^*}{\gamma^*} \sqrt{\frac{2 \cdot \pi \cdot \tilde{R} \cdot T}{\tilde{M}}} \cdot \frac{\lambda_g}{p \cdot \left(2 \cdot c_{p,g} - \frac{\tilde{R}}{\tilde{M}} \right)}, \tag{A.3}$$

where $\tilde{R}$ represents the gas constant and $\tilde{M}$ the molar mass of the gas. The accommodation coefficient γ^* can be calculated for air with [34]:

$$\log \left(\frac{1}{\gamma^*} - 1 \right) = 0.6 - \frac{\frac{1000\ \mathrm{K}}{T_g} + 1}{2.8}. \tag{A.4}$$

The radiation is described through:

$$\alpha_{rad} = 4 \cdot C_{12} \cdot T^3 \text{ and } C_{12} = \sigma \cdot \frac{1}{\frac{1}{\varepsilon_w} + \frac{1}{\varepsilon_s} - 1}, \tag{A.5}$$

with σ denoting the Stefan-Boltzmann constant and ε_i the emissivity of the respective surface.

A.2. Calculation of the measurement uncertainty

To determine the uncertainty of the measurements, the procedure proposed by the ISO is followed. The approach is given in the guideline expression of uncertainty in measurement (GUM) [33] and the definitions will be shortly summarized below.

Consider a measurand Y, which is a function of the measured quantities $X_1, \ldots, X_N$:

$$Y = f(X_1, \ldots, X_N). \tag{A.6}$$

The estimate of the measurand Y is defined as y and the estimate of the quantity X_i as x_i. The standard deviation of y can be calculated by taking the standard uncertainties of its input estimates x_i:

$$u(y) = \sqrt{\sum_{i=1}^{N} \left(\frac{\partial f}{\partial x_i} \right)^2 u^2(x_i)}. \tag{A.7}$$

With this, the uncertainty of the measurand can be calculated. The derivatives $\partial f / \partial x_i$ are the sensitivity coefficients and describe the change of the output with changes in the input quantities.

The first step for calculating the uncertainty of the measured heat transfer coefficient is the derivation of it according to the parameters. The written-out coefficient is given as:

$$\alpha_{ws} = \frac{m_s \cdot c_{p,s} \cdot (T_{s2} - T_{s1})}{A_{ws} \cdot \left(\bar{T}_w - \bar{T}_s \right) \cdot (t_2 - t_1)} + \frac{\left(\sigma \cdot T_{TC,1}^4 - J_s \right) \cdot A_{s,rad}}{\left(\frac{1-\varepsilon_s}{\varepsilon_s} \right) \cdot A_{ws} \cdot \left(\bar{T}_w - \bar{T}_s \right)}, \tag{A.8}$$

and is a function of 13 parameters. Considering that the radiosity J_s is a function of the cylinder temperatures opposite to the bed $T_{w,rad}$, at the front T_f and the back T_b, this number rises to 16 parameters.

Exemplarily, the results obtained for the case with sand at a filling of 10 % and at 1 rpm will be discussed. For the calculation of the uncertainty of the heat transfer coefficient, the uncertainties associated with the respective parameters are needed. The input mass for the experiments was weighed with a high-precision scale. The extended uncertainty of the scale $U(m)$ is given as ±0.008 g, with a confidence interval of 95 %. The standard uncertainty $u(m)$ is therefore ±0.004 g according to [33]. Deviations in the mass will also affect the calculated bed height and surfaces. However, since the bed masses were in the range of 1–3.5 kg, this uncertainty is neglected. The time measurement is performed in the experiments every second, thus having an uncertainty of ±0.5 s. Assuming that the measured time has a zero probability of lying outside this interval, a rectangular distribution is taken which results in [33]:

$$u(t) = \frac{0.5\ \mathrm{s}}{\sqrt{3}} = 0.29\ \mathrm{s}. \tag{A.9}$$

The biggest impact is expected by the accuracy of the thermocouples. To assess the uncertainty of the thermocouples, the factory tolerance indicated as class 2 is used. The tolerance of the class is given as ±2.5 K or $0.0075 \cdot |T\ \text{in}^\circ\mathrm{C}|$, with the higher value to be taken. Again, a rectangular distribution is considered for the temperature measured by a single thermocouple and thus it follows for the uncertainty:

$$u(T_{TC}) = \frac{2.5\ \mathrm{K}}{\sqrt{3}} = 1.44\ \mathrm{K}. \tag{A.10}$$

Table A.1
Standard uncertainties associated with experimental parameters.

Parameter	Standard uncertainty u
$c_{p,s}$	0.204 J/(kg K) at 20°C 0.068 J/(kg K) at 120°C
m_s	0.004 g
T_{TC}	1.44 K
T_s	0.49 K
$\bar{T}_s$	0.22 K
T_w	0.83 K
$\bar{T}_w$	0.37 K
t	0.29 s

All remaining parameters of the heat transfer coefficient are based on other measurands and require the determination of their uncertainties according to Eq. (A.7). Exceptions to this are the emissivities, which are mainly taken from the literature and neglected in the analysis.

After defining the uncertainty of a single thermocouple, the corresponding value for the averaged bed temperature can be obtained. For this, the respective areas enclosed by the thermocouples are considered. The uncertainty for the bed temperature measured by 9 thermocouples is calculated as:

$$u(T_s) = 0.49 \text{ K}. \tag{A.11}$$

The average bed temperature $\bar{T}_s$ in the considered time interval is the average of the taken measurements N. The averaging is done over 5 measurements at a rotational speed of 1 rpm. Since all values have the same uncertainty, Eq. (A.7) simplifies in this case to:

$$u\left(\bar{T}_s\right) = \frac{u(T_s)}{\sqrt{N}}, \tag{A.12}$$

and with $N = 5$ it follows:

$$u\left(\bar{T}_s\right) = 0.22 \text{ K}. \tag{A.13}$$

Furthermore, the wall temperatures are obtained with a fit through all three plates A–C. With the same approach as above the uncertainty is:

$$u(T_w) = \frac{u(T_{TC})}{\sqrt{3}} = 0.83 \text{ K}, \tag{A.14}$$

and subsequently for the interval of 5 measurements:

$$u\left(\bar{T}_w\right) = 0.37 \text{ K}. \tag{A.15}$$

The uncertainty of the specific heat has to be determined at the respective average temperature of the bed in the time interval. For the sand, the uncertainty in the total temperature range of 20 and 120 °C is given as:

$$u\left(c_{p,s,20^\circ C}\right) = 0.204 \ \frac{\text{J}}{\text{kg K}}, \tag{A.16}$$

$$u\left(c_{p,s,120^\circ C}\right) = 0.068 \ \frac{\text{J}}{\text{kg K}} \ . \tag{A.17}$$

Considering that the actual value of the specific heat at these temperatures is in the order of 800 J/(kg K), no significant impact of this parameter is to be expected. The before calculated uncertainties are summarized in Table A.1.

After applying these values to the experimental case with sand, filling of 10 %, 1 rpm and at 40 °C a standard uncertainty of ±6.7 % is obtained. The uncertainty was found to be the highest in the beginning and end of the experiment, with about ±10 %, due to lower temperature differences. Thus, the uncertainty of the thermocouples increases in importance, when the difference decreases. Overall, the uncertainties were below ±10 % in most cases, with few being in the range of ±15 %. It is worth mentioning, that a positive mitigating impact of the averaging of thermocouples and measurements at each plate was found on the uncertainty.

References

[1] A.A. Boateng, Rotary Kilns: Transport Phenomena and Transport Processes, Elsevier Science, 2008.
[2] B. Andreotti, Y. Forterre, O. Pouliquen, Granular Media: Between Fluid and Solid, Cambridge University Press, 2013.
[3] IEA, Energy Technology Perspectives 2020. 2020.
[4] Olivier, J.G.J., et al., Trends in global CO2 emissions: 2016 Report. 2016, Ispra: European Commission, Joint Research Centre: The Hague: PBL Netherlands Environmental Assessment Agency.
[5] P. Barr, J. Brimacombe, A. Watkinson, A heat-transfer model for the rotary kiln: Part I. Pilot kiln trials, Metallurg. Mater. Trans. B 20 (3) (1989) 391–402.
[6] J. Gorog, T. Adams, J. Brimacombe, Regenerative heat transfer in rotary kilns, Metallurg. Trans. B 13 (2) (1982) 153–163.
[7] A. Watkinson, J. Brimacombe, Heat transfer in a direct-fired rotary kiln: II. Heat flow results and their interpretation, Metallurg. Trans. B 9 (2) (1978) 209–219.
[8] E. Alonso, M. Romero, Review of experimental investigation on directly irradiated particles solar reactors, Renew. Sustain. Energy Rev. 41 (2015) 53–67.
[9] G. Moumin, et al., Solar treatment of cohesive particles in a directly irradiated rotary kiln, Solar Energy 182 (2019) 480–490.
[10] E. Alonso, et al., Use of rotary kilns for solar thermal applications: Review of developed studies and analysis of their potential, Solar Energy 144 (2017) 90–104.
[11] H. Henein, J. Brimacombe, A. Watkinson, Experimental study of transverse bed motion in rotary kilns, Metallurg. Trans. B 14 (2) (1983) 191–205.
[12] L. Wachters, H. Kramers, The calcining of sodium bicarbonate in a rotary kiln, in: Proceedings of 3rd European Symposium Chemical Reaction Engineering, 1964.
[13] D. Pashkevich, et al., Heat exchange of dynamic powder beds with a heat–transfer surface. I. a helical screw conveyer and a horizontal rotating cylinder, J. Eng. Phys. 72 (1) (1999) 1–6.
[14] A.S.B. Njeng, et al., Wall-to-solid heat transfer coefficient in flighted rotary kilns: experimental determination and modeling, Exper. Thermal Fluid Sci. 91 (2018) 197–213.
[15] S. Tscheng, A. Watkinson, Convective heat transfer in a rotary kiln, Can. J. Chem. Eng. 57 (4) (1979) 433–443.
[16] E.-U. Schlünder, Heat transfer to packed and stirred beds from the surface of immersed bodies, Chem. Eng. Process.: Process Intensif. 18 (1) (1984) 31–53.
[17] W. Sullivan, R. Sabersky, Heat transfer to flowing granular media, Int. J. Heat Mass Transf. 18 (1) (1975) 97–107.
[18] J. Lehmberg, M. Hehl, K. Schügerl, Transverse mixing and heat transfer in horizontal rotary drum reactors, Powder Technol. 18 (2) (1977) 149–163.
[19] S.Q. Li, et al., A Mathematical Model of Heat Transfer in a Rotary Kiln Thermo-Reactor, Chem. Eng. Technol. 28 (12) (2005) 1480–1489.
[20] E.-U. Schlünder, N. Mollekopf, Vacuum contact drying of free flowing mechanically agitated particulate material, Chem. Eng. Process.: Process Intensif. 18 (2) (1984) 93–111.
[21] G. Wes, A. Drinkenburg, S. Stemerding, Heat transfer in a horizontal rotary drum reactor, Powder Technol. 13 (2) (1976) 185–192.
[22] F. Herz, et al., Influence of the motion behavior on the contact heat transfer between the covered wall and solid bed in rotary kilns, Exper. Heat Transf. 28 (2) (2015) 174–188.
[23] Y. Sonavane, Influence of the wall on the heat transfer process in rotary kiln, 2010.
[24] C.E. Wicks, F.E. Block, Thermodynamic Properties of 65 Elements: Their Oxides, Halides, Carbides and Nitrides, 605, US Government Printing Office, 1963.
[25] B. Kohlhaas, O. Labahn, Cement engineers' handbook, Bauverlag, 1983.
[26] F. Herz, Y. Sonavane, E. Specht, Analysis of local heat transfer in direct fired rotary kilns, 14th International Heat Transfer Conference, American Society of Mechanical Engineers Digital Collection, 2010.
[27] F. Herz, et al., Influence of operational parameters and material properties on the contact heat transfer in rotary kilns, Int. J. Heat Mass Transf. 55 (25–26) (2012) 7941–7948.
[28] F. Herz, et al., Experimental study of the contact heat transfer coefficient between the covered wall and solid bed in rotary drums, Chem. Eng. Sci. 82 (2012) 312–318.
[29] A.I. Nafsun, et al., Heat transfer experiments in a rotary drum for a variety of granular materials, Exper. Heat Transf. 29 (4) (2016) 520–535.
[30] A. Nafsun, F. Herz, The effect of solid bed dispersity on the contact heat transfer in rotary drums, 12th International Conference on Heat Transfer, Fluid Mechanics and Thermodynamics, 2016.
[31] A.I. Nafsun, Experimental Analysis of Heat Transport in the Solid Bed of Rotary Kilns, docupoint GmbH, 2016.
[32] T.L. Bergman, et al., Fundamentals of Heat and Mass Transfer, Wiley, 2017.
[33] ISO, International Organization for Standardization. Evaluation of measurement data — Guide to the expression of uncertainty in measurement. 2008 [cited 2020 January 8th]; Available from: https://www.iso.org/sites/JCGM/GUM/JCGM100/C045315e-html/C045315e.html.
[34] H. Martin, Wärme- und Stoffübertragung in der Wirbelschicht, Chemie Ingenieur Technik 52 (3) (1980) 199–209.